FTIR Study of the Oxidation of Porous Silicon

Douglas B. Mawhinney, John A. Glass, Jr., and John T. Yates, Jr.*

Surface Science Center, Department of Chemistry, University of Pittsburgh, Pittsburgh, Pennsylvania 15260

Received: October 25, 1996; In Final Form: December 16, 1996[⊗]

The oxidation of hydrogen-terminated porous silicon surfaces produced by electrochemical etching has been studied using transmission FTIR spectroscopy. The surface is passivated to oxidation by surface hydrogen below about 523 K. Above this temperature as hydrogen depletion occurs by H_2 evolution, Si surface dangling bond sites, capable of O_2 dissociation, are involved in initiating the first stage of oxidation. Two reactions are observed. The first, O insertion into Si−Si back-bonds, leads to $-O_ySiH_x$ surface species which exhibit frequency shifts to the blue compared to parent SiH_x stretching modes. In addition, Si−O−Si modes are also observed to form. The second reaction involves oxygen atom insertion into Si−H bonds to produce isolated Si−OH surface species.

Introduction

The oxidation of silicon has been thoroughly studied on silicon single crystal surfaces.[1,2] Highly controlled silicon dioxide insulating layers are used for barrier junctions in electronic devices as well as for surface passivation in silicon device processing. Vibrational spectroscopic studies of the oxidation process were conducted on silicon single crystals using analytical techniques such as high-resolution electron energy loss spectroscopy (HREELS)[3] or internal reflection infrared spectroscopy.[4,5] This investigation focuses on the oxidative behavior of porous silicon, studied by transmission FTIR spectroscopy.

Porous silicon has gained much interest[6−10] since the discovery of its light-emission characteristics[11] under optical and electrical excitation. Controlling the emission wavelength, which is dependent on surface modification[7,12−15] as well as applied bias,[14] is a much sought after goal. This ability to control the wavelength output of porous silicon would allow its incorporation into optoelectronic devices such as flat panel displays. Some porous silicon devices have already been demonstrated.[16]

Another attractive feature of porous silicon is the enhancement in surface area created by the etching process. Adsorption isotherm studies show a surface area of ∼200 m^2/cm^3 for porous silicon etched on p-type Si(100).[17] Given typical porous silicon layer depths of 3−6 μm, a porous layer geometrical area of 1 cm^2, and a site density of 6.8×10^{14} sites/cm^2 for Si(100),[18,19] a new site density of $\sim 10^{18}$ sites/cm^2 can be calculated for the porous silicon layer.

This gives porous silicon enough surface area to allow surface reactions to be monitored by transmission infrared spectroscopy. This technique not only gives better frequency resolution than HREELS, but also can be used to observe surface reactions at much higher gas pressure than the electron spectroscopies. Because of the random orientation of the porous surface, transmission FTIR is carried out with unpolarized light and does not utilize the selection rules related to the orientation of the surface dipoles.

The focus of earlier research on the oxidation of porous silicon has been on mass changes,[20] oxidation under wet conditions,[20,21] and the study of the shifting of the Si−H stretching modes[21−23] as oxidation progresses.

This frequency shift has been explained by an induction theory.[24,25] The insertion of more electronegative atoms into silicon back-bonds will cause a reduction of the Si−H bond length as the electronegative atom pulls electron density away from silicon and hydrogen. This produces an increase of the bond strength of the Si−H bond, which is caused by an increase of the σ-character of the Si−H bond. This increase of bond strength associated with σ-bond character results in an increase of the degree of steepness in the vibrational potential well walls, which results in an increase in the Si−H stretching frequency. The induction theory has been shown to apply for gas phase molecules.[23]

This paper deals with surface modifications due to the oxidation process that can be be monitored by transmission FTIR spectroscopy. Evidence is presented for the formation of three surface species: (SiOSi), ($-O_ySiH_x$), and (SiOH). Monitoring the formation sequence of these surface species allows the extent of oxidation to be measured. Isotopic studies involving D_2, $^{16}O_2$, and $^{18}O_2$ provide mechanistic information on the oxidation as well as a differentiation between surface and bulk oxide modes.

Experimental Section

Vacuum System. The stainless steel vacuum system is pumped sequentially with a liquid N_2 cooled zeolite sorption pump, a Pfeiffer-Balzers 50 L/s turbomolecular pump, and a Varian 20 L/s ion pump. The system has a base pressure of 1×10^{-7} Torr, which can be reached after 20 h of baking while pumping. The background pressure is measured by both the ion pump current and an ionization gauge. Gas pressures are measured with an MKS capacitance manometer with a range from 1×10^{-3} to 1000 Torr. The system is also equipped with a UTI 100C quadrupole mass spectrometer for residual gas analysis and for helium leak detection.

The sample cell used in these experiments is illustrated in Figure 1 and has been described previously.[26,27] The stainless steel cell is used at pressures from $\sim 10^{-8}$ to ∼760 Torr. The sample can be rotated 360° about the vertical axis, allowing it to be moved out of the infrared path for spectral measurement of the background. The sample is held in place by tantalum foil electrical connections that connect via tungsten extensions to a feedthrough. The power leads and type K thermocouple leads pass through a liquid N_2 cooled Dewar and connect to a 0−50 A, 0−100 V power supply controlled by a Honeywell UDC 500 digital controller. This setup allows temperature

[⊗] Abstract published in *Advance ACS Abstracts,* February 1, 1997.

S1089-5647(96)03322-6 CCC: $14.00

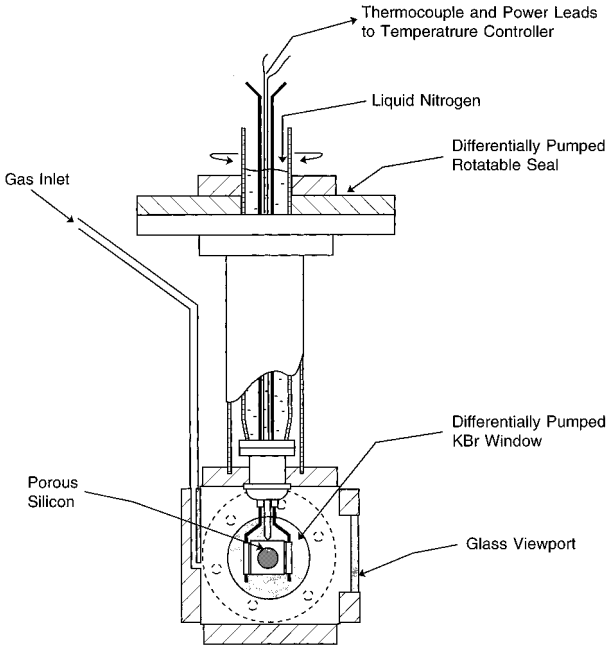

Figure 1. Drawing of infrared cell containing a porous silicon layer on a silicon (100) single crystal.

control from 108 to 900 K with an accuracy of ±1 K via feedback from the type K thermocouple inserted into a tantalum envelope wedged into a slot on the top of the crystal. The cell is also equipped with differentially pumped KBr infrared windows.

Materials. Si(100) p-type, B-doped, 5−10 Ω cm crystals were obtained from Virginia Semiconductors, Inc. The crystals measured 1.3 × 1.3 × 0.15 cm thick and were slotted 0.1 cm deep on all four edges to allow insertion of the tantalum electrical connectors and the tantalum envelope which separated the thermocouple from the crystal. All crystals were cleaned by the RCA procedure[28] before the etching process. The crystals were anodically etched in a deoxygenated aqueous solution of 48% HF(aq) and anhydrous ethanol. A dc current of 100 mA was applied with a Hewlett-Packard E3612A power supply for 25 s to produce a hydrogenated porous layer of 0.75 cm^2 geometrical area. The etched crystal was dipped in 48% HF-(aq) to remove any surface oxide and residual etching solution before being mounted into the infrared cell.

Research grade $^{16}O_2$ with a purity of 99.998% was obtained from Matheson. The gas was transferred directly from the cylinder to the gas line for introduction into the sample cell.

Isotopic oxygen ($^{18}O_2$) was obtained from ICON Services, Inc. The gas had an isotopic purity of 95 atom %. The gas was transferred from the glass bulb to the gas line for introduction into the sample cell.

D_2 was obtained from Matheson. The gas had an isotopic purity of 99.82 atom %. The gas was transferred from the glass bulb to the gas line for introduction to the sample cell.

IR Measurements. All spectra were measured with a Mattson Research Series I FTIR spectrometer. The spectrometer employed a liquid N_2 cooled HgCdTe detector, sensitive to the infrared region from 4000 to 500 cm^{-1}. All spectra were recorded at 2 cm^{-1} resolution and averaged using 1024 scans. The spectrometer was controlled from a personal computer using WinFIRST software supplied by Analytical Technology, Inc.

Results

Porous Silicon Layer Prepared on Si(100). An infrared spectrum measured at 298 K of an unetched Si(100) crystal

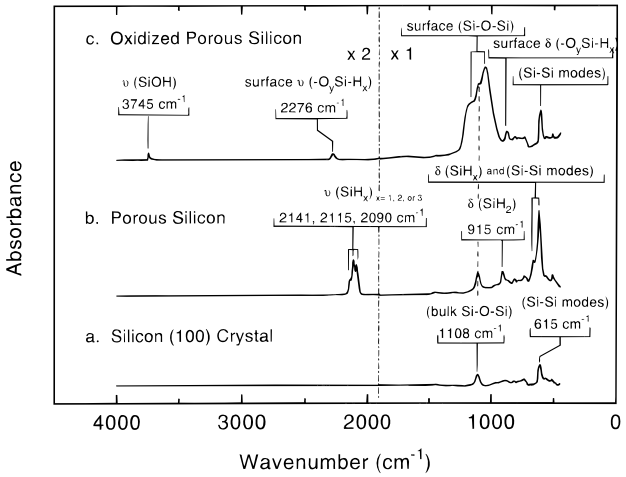

Figure 2. Spectra taken at 298 K of three different stages of surface modification: (a) Si(100), (b) porous silicon on Si(100), and (c) oxidized porous silicon on Si(100).

(Figure 2a) reveals the presence of various silicon crystal modes as well as a Si−O−Si mode at 1108 cm^{-1}. After electrochemical etching (Figure 2b) a number of new absorbances appear in the spectrum. The absorbances at 2141, 2115, and 2090 cm^{-1} are attributed respectively to SiH_x (x = 3, 1, 2) stretching modes.[29] At lower wavenumbers, the Si−O−Si absorbance at 1108 cm^{-1} is still present, as well as new features such as the SiH_2 scissor mode at 915 cm^{-1}, and various SiH_x deformation modes overlapping the silicon crystal modes which are observed at 666, 622, and 615 cm^{-1}. Figure 2c shows the spectral changes produced after heavy oxidation of the porous silicon. New vibrational modes due to Si−OH, $-O_ySiH_x$, and surface Si−O−Si species are observed and will be discussed in more detail later.

Partially Oxidized Porous Silicon. The first evidence of oxidation occurs at 523 K under an O_2 pressure of 0.2 Torr, as seen by modification of the frequency of the SiH_x modes. The oxidation becomes much more evident by 573 K (Figure 3A, spectrum b), as seen by an intensity decrease of the various SiH_x stretching modes, the growth of a broad absorbance band centered at approximately 2160 cm^{-1}, and the development and shift of SiH_x absorbances in the regions near 2254 and 2199 cm^{-1}. Simultaneously, a broad band near the existing bulk Si−O−Si mode at 1108 cm^{-1} begins to grow with a maximum at 1050 cm^{-1} (not shown), and in the lower frequency regions, the SiH_2 scissor and SiH_x deformation modes begin to diminish in absorbance (not shown). Also, an SiOH absorbance begins to develop at approximately 3736 cm^{-1} with a broad tail extending to lower frequencies (Figure 4).

Heavily Oxidized Porous Silicon. As the oxidation proceeds to completion, absorbances develop at 2214 and 2273 cm^{-1} while the original SiH_x stretching modes disappear completely (Figure 3B). The 3736 cm^{-1} mode increases in intensity (Figure 4), as well as the broad band with a maximum at 1050 cm^{-1} (not shown). At lower frequencies, a new absorbance at 877 cm^{-1} with a shoulder at 841 cm^{-1} appears (not shown). Also, a silicon crystal mode becomes visible again at 615 cm^{-1} as a result of the disappearance of δ(Si−H_x) modes.

Completing the oxidation process under 760 Torr of O_2 and cooling to 298 K leaves new absorbance peaks at 3745, 2276, 1168, and 1050 cm^{-1} (Figure 2c) and at 881 cm^{-1}(Figures 2c and 5). Also present are a silicon crystal mode at 615 cm^{-1} and a bulk Si−O−Si mode at 1108 cm^{-1}.

Studies Using Isotopic $^{18}O_2$ and D_2. Oxidation at 650 K performed with 33 Torr of $^{18}O_2$ produced the isotopic mass-

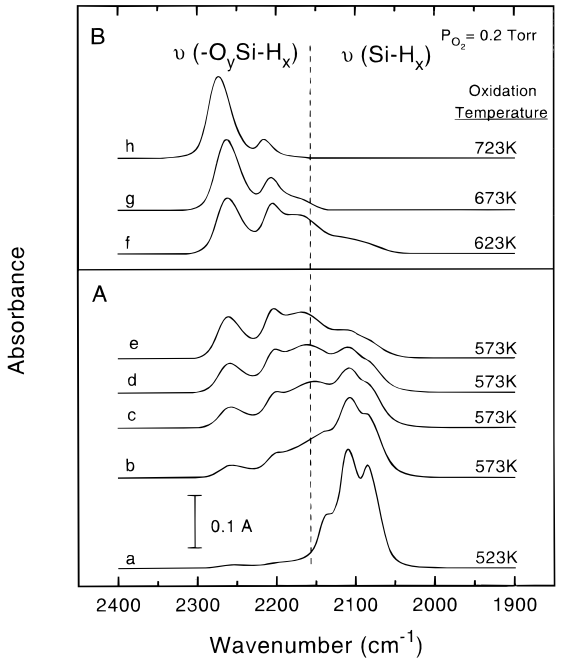

Figure 3. (A) Early stages of oxidation as noted by development of oxidized silicon−hydride stretching bands. (B) Continued growth and shifting of the oxidized silicon−hydride stretching bands as the oxidation temperature is raised.

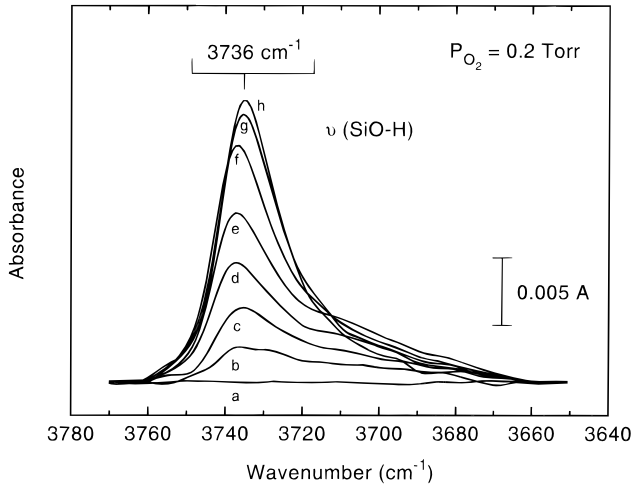

Figure 4. SiO−H stretching mode development (smoothed data). The reaction conditions for each lettered spectrum correspond to the same conditions as each lettered spectrum in Figure 3A,B.

TABLE 1: Observed Frequency Shifts (cm^{-1}) between $^{16}O_2$ and $^{18}O_2$ Oxidation

	υ(SiO−H)	υ(−O_ySi−H_x)	υ(Si−O−Si)	υ(Si−O−Si)	δ(−O_ySi−H_x)
^{16}O	3747	2273	1176	1065	881
^{18}O	3736	2271	1121	1015	876

affected frequencies, measured at 108 K, listed in Table 1 (Figures 5 and 6).

Oxidation of hydrogenated (H) porous silicon, performed at 650 K with 3 Torr of D_2 and 30 Torr of $^{16}O_2$, showed no evidence of Si−OD formation (Figure 7).

Discussion

Spectral Shifts for Silicon Hydride Modes during Oxidation. The oxidation process on hydrogen passivated porous silicon begins near 523 K under an oxygen pressure of 0.2 Torr. This threshold temperature for oxidation corresponds to the appearance of oxygen modified hydride stretching modes at

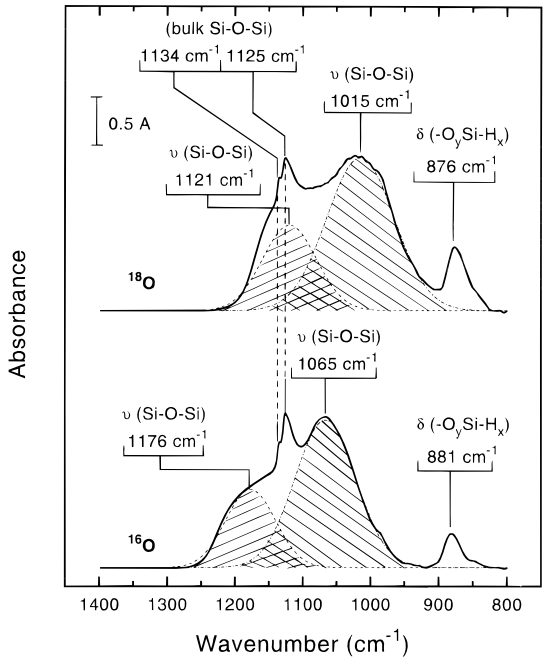

Figure 5. Si−O−Si asymmetric stretch, bulk oxide modes, and oxidized silicon−hydride deformation mode measured at 108 K after oxidation with $^{16}O_2$ or $^{18}O_2$. The cross-hatched absorbance bands indicate the two asymmetric Si−O−Si modes formed by surface oxidation. Fitting was performed with Microcal Origin software. The slight difference in ^{16}O frequencies in the Si−O−Si region here compared to those seen in Figure 2 are due to temperature differences during the spectral measurements.

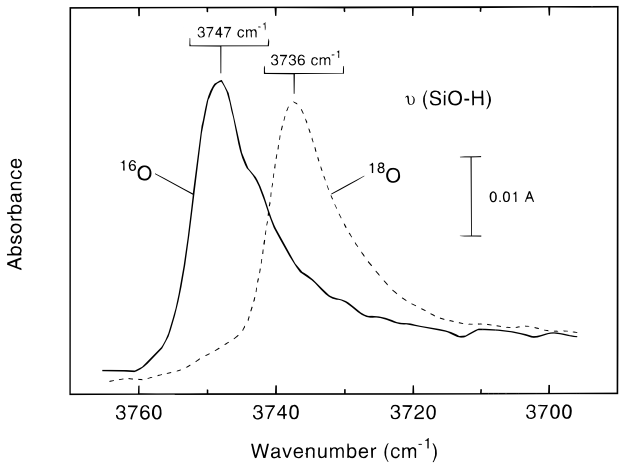

Figure 6. Isotopic frequency of the SiO−H stretch after oxidation with $^{18}O_2$, compared to the same mode after $^{16}O_2$ oxidation. The 11 cm^{-1} difference in ^{16}O frequencies in the isolated SiO−H stretch here compared to those seen in Figure 4 are due to temperature differences during the spectral measurements.

higher frequencies compared to those for SiH_x ($x = 1-3$) species. This oxidation threshold temperature coincides closely with the temperature of hydrogen desorption from porous silicon as reported elsewhere,[30] which exposes silicon dangling bonds that can adsorb oxygen.

An induction theory developed to explain the SiH_x shifting phenomenon[24,25] notes that substitution of electronegative atoms into silane causes the hydride stretching modes to shift to higher frequencies. In the case of hydrogenated porous silicon, the general upward frequency shift in the υ(−O_ySi−H_x) mode with increasing oxidation is due to an increasing degree of back-bonding to oxygen, progressing toward the $-O_3SiH$ species. Similar oxidized porous silicon hydride surface species have been proposed by others.[3,20−22,31]

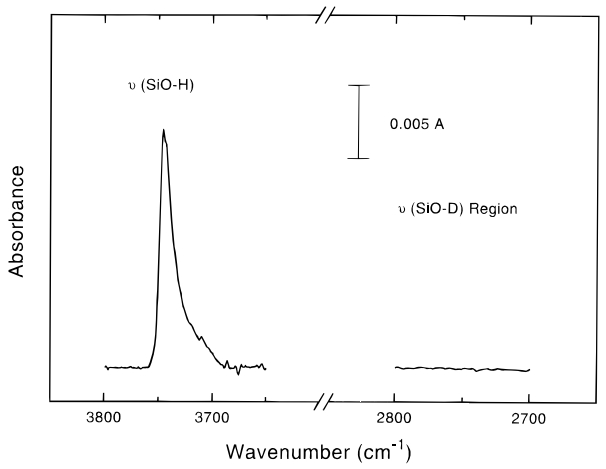

Figure 7. Spectra showing SiO−H stretch and lack of SiO−D stretch after oxidation with 33 Torr of $^{16}O_2$ and 3 Torr of D_2, demonstrating the absence of D_2O formation and decomposition on the surface.

The assignment of the 881 cm^{-1} band as an oxidized hydride deformation mode, $\delta(-O_ySi-H_x)$, warrants further discussion because other researchers studying silicon oxidation have assigned absorbances in this region to stretching modes of various oxide species, Si_xO_y ($x = 2-4$, $y = 5 - x$).[20,32] However, evidence in favor of our assignment comes from the $^{18}O_2$ oxidation experiment. The resultant shift for the Si−O−Si stretch was ∼−50 cm^{-1}; while the 881 cm^{-1} peak shifted only by −5 cm^{-1}. The magnitude of difference between the two shifts can be explained by ^{18}O having a primary isotopic mass effect on the Si−O−Si mode, compared to a secondary mass effect of the same oxygen on the hydride mode.

Formation of Surface Si−O−Si Species. The crystals used in this study contained oxide in the bulk, as evidenced in the 1108 cm^{-1} absorbance in Figure 2a. As oxidation proceeds, a broad absorbance attributed to asymmetric stretching modes of SiO_2[33,34] begins to appear at frequencies on either side of this bulk mode. The added absorbance grows throughout the oxidation process and eventually covers the region from 1250 to 950 cm^{-1}, but never merges with the 1108 cm^{-1} band. Also, the 1108 cm^{-1} band fails to shift with $^{18}O_2$ oxidation, showing that it is not related to the surface oxidation process.

Since these two bands never merge, they must correspond to two different forms of oxide. The growth of the absorbances in the region from 1250 to 950 cm^{-1} corresponds to the growth of a layer of amorphous SiO_2, while the 1108 cm^{-1} results from an oxygen atom bound in the bulk of the original silicon crystal. Furthermore, the absence of the broad absorbance features in the 1250−950 cm^{-1} region before oxidation suggests that little surface oxide exists on the electrochemically etched porous silicon surface.

Formation of Various SiOH Species. The various SiOH species have been well studied on silica surfaces.[35−38] The oxidation process on porous silicon creates at least two types of SiOH species, specifically isolated and associated SiOH.

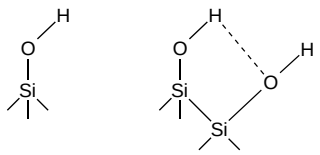

I **II** and **III**

The spectral signature for associated Si−OH groups are O−H stretching modes with low frequency due to hydrogen-bonding effects[39] compared to those of isolated Si−OH groups. Thus, the spectral development of the SiO−H modes, shown in Figure 4, proceeds from low-intensity spectra exhibiting strong relative intensity of associated Si−OH species (∼3701 cm^{-1}) to a high-intensity spectrum in which most of the SiO−H modes appear to originate from isolated Si−OH groups (∼3736 cm^{-1}).

During surface oxidation, a constant initial number of SiH_x species are being converted to $-O_ySiH_x$ species and Si−OH species as more and more surface oxide is produced by increased oxidation of the porous silicon as the temperature and exposure to O_2 are increased. The increase in the surface area of SiO_2, accompanied by a constant initial supply of SiH_x species to produce Si−OH species, would logically lead to the production of an increasing fraction of isolated Si−OH species as oxidation progresses and as associated Si−OH species convert to isolated Si−OH species. This is in agreement with the changes of the IR spectrum in the SiO−H stretching region as shown in Figure 4.

Three possible routes could lead to the formation of the surface silanol species produced during oxidation, where the equations denote bond character rather than known surface species.

1. Si−O bonds and Si−H bonds react to form the surface silanol:

$$Si-H + Si-O \rightarrow SiOH + Si$$

2. Water desorbed from the walls of the cell during heating decomposes on the clean silicon surface sites produced above ∼523 K:[21,40]

$$H_2O + Si \rightarrow Si-OH + Si-H$$

3. Desorbing hydrogen reacts with reactant oxygen in the cell to form water. This water then decomposes on the clean silicon surface sites produced above ∼523 K:

$$H_2O + Si \rightarrow Si-OH + Si-H$$

Reaction pathway 2 is disproved by the data from the oxidation experiment with $^{18}O_2$. Vibrational modes due to Si−^{16}OH species would have been observed if this process occurred to a significant extent. However, the results shown in Figure 6 indicate that ^{18}O was incorporated into all of the SiOH species on the surface.

A second control experiment disproved reaction pathway 3. Oxidation performed with a D_2 pressure of 3 Torr showed no SiO−D formation by lack of any vibrational mode in the proximity of 2648 cm^{-1}.

The route to isolated Si−OH species therefore must be related to pathway 1 shown above. At temperatures above about 523 K, SiH_x species begin to decompose producing H_2,[30] leaving Si surface dangling bond sites that react with O_2 to produce Si−O bonds. The insertion of O into Si−H bonds then begins to occur, producing Si−OH species which are observed by their characteristic IR spectrum.

Conclusions

The oxidation of hydrogenated porous silicon has been studied by transmission FTIR spectroscopy. The following results were obtained:

1. Oxidation occurs at a threshold temperature near 523 K where the first evidence for loss of hydrogen from the surface is observed by IR spectroscopy. The Si dangling bond sites produced are able to chemisorb O_2 dissociatively, leading to the first stage of surface oxidation.

2. Oxidation leads to O insertion into Si−Si back-bonds, producing $-O_ySiH_x$ species. The Si−H stretching frequencies of these species are characterized by 150−200 cm^{-1} upward frequency shifts compared to SiH_x species as a result of enhanced Si−H σ-bond character caused by electron withdrawal by the oxygen moieties.

3. Oxidation also leads to the formation of surface Si−OH species as a result of O insertion into Si−H bonds. As the degree of oxidation increases, a single SiO−H mode observed near 3736 cm^{-1} develops. This mode is indicative of the formation of isolated Si−OH species, a natural consequence of the limited number of Si−H bonds available in comparison to an increasing number of Si−O−Si bonds produced as oxidation increases.

4. The formation of Si−O−Si modes, originating from oxidation of the porous silicon surface, produces absorbance frequencies near 1176 and 1065 cm^{-1}. These modes are distinct from Si−O−Si modes at 1134 and 1125 cm^{-1} which originate from oxygen initially present in the bulk of the silicon.

Acknowledgment. We thank Patrick Maley for his assistance at the beginning of the project and Edward A. Wovchko for many useful discussions about the vibrational spectra of silica. We also thank the Office of Naval Research for their support of this work through an AASERT grant.

References and Notes

(1) Ibach, H.; Horn, K.; Dorn, R.; Lüth, H. *Surf. Sci.* **1973,** *38*, 433.
(2) Engel, T. *Surf. Sci. Rep.* **1993,** *18*, 91.
(3) Schaefer, J. A.; Frankel, D.; Stucki, F.; Göpel, W.; Lapeyre, G. J. *Surf. Sci.* **1984,** *139*, L209.
(4) Zazzera, L.; Evans, J. F. *J. Vac. Sci. Technol. A* **1993,** *11*, 934.
(5) Niwano, M.; Kageyama, J.; Kinashi, K.; Miyamoto, N.; Honma, K. *J. Vac. Sci. Technol. A* **1994,** *12*, 465.
(6) Xie, Y.-H.; Wilson, W. L.; Ross, F. M.; Mucha, J. A.; Fitzgerald, E. A.; Macaulay, J. M.; Harris, T. D. *J. Appl. Phys.* **1992**, *71*, 2403.
(7) Iyer, S. S.; Xie, Y.-H. *Science* **1993**, 260, 40.
(8) Canham, L. *MRS Bull.* **1993** (July), 22.
(9) Prokes, S. M. *J. Mater. Res.* **1996**, *11*, 305.
(10) Hamilton, B. *Semicond. Sci. Technol.* **1995**, *10*, 1187.
(11) Canham, L. T. *Appl. Phys. Lett.* **1990**, *57*, 1046.
(12) Brus, L. *J. Phys. Chem.* **1994**, *98*, 3575.
(13) Wang, S.-Y.; Shen, W.-Z.; Shen, X.-C.; Zhu, L.; Ren, Z.-M.; Li, Y.-F.; Liu, K.-F. *Appl. Phys. Lett.* **1995**, *67*, 783.
(14) Bsiesy, A.; Hory, M. A.; Gaspard, F.; Herino, R.; Ligeon, M.; Muller, F.; Romestain, R.; Vial, J. C. *Microelectron. Eng.* **1995**, *28*, 233.
(15) Tischler, M. A.; Collins, R. T.; Stathis, J. H.; Tsang, J. C. *Appl. Phys. Lett.* **1992**, *60*, 639.
(16) Araki, M.; Koyama, H.; Koshida, N. *Jpn. J. Appl. Phys., Part 1* **1996**, *35*, 1041.
(17) Bomchil, G.; Herino, R.; Barla, K.; Pfister, J. C. *J. Electrochem. Soc.* **1983**, *130*, 1611.
(18) Cheng, C. C.; Yates, Jr., J. T. *Phys. Rev. B* **1991**, *43*, 4041.
(19) Lu, Z. H.; Griffiths, K.; Norton, P. R.; Sham, T. K. *Phys. Rev. Lett.* **1992**, *68*, 1343.
(20) Unagami, T. *Jpn. J. Appl. Phys.* **1980**, *19*, 231.
(21) Ogata, Y.; Niki, H.; Sakka, T.; Iwasaki, M. *J. Electrochem. Soc.* **1995**, *142*, 1595.
(22) Kato, Y.; Ito, T.; Hiraki, A. *Jpn. J. Appl. Phys.* **1988**, *27*, L1406.
(23) Gupta, P.; Dillon, A. C.; Bracker, A. S.; George, S. M. *Surf. Sci.* **1991**, *245*, 360.
(24) Lucovsky, G. *Solid State Commun.* **1979**, *29*, 571.
(25) Borghesi, A.; Guizzetti, G.; Sassella, A.; Bisi, O.; Pavesi, L. *Solid State Commun.* **1994**, *89*, 615.
(26) Basu, P.; Ballinger, T. H.; Yates, Jr., J. T. *Rev. Sci. Instrum.* **1988**, *59*, 1321.
(27) Glass, Jr., J. A.; Wovchko, E. A.; Yates, Jr., J. T. *Surf. Sci.* **1995**, *338*, 125.
(28) Kern, W.; Puotinen, D. A. *RCA Rev.* **1970**, *31*, 187.
(29) Glass, Jr., J. A.; Wovchko, E. A.; Yates, Jr., J. T. *Surf. Sci.* **1996**, *348*, 325.
(30) Gupta, P.; Colvin, V. L.; George, S. M. *Phys. Rev. B* **1988**, *37*, 8234.
(31) Morterra, C.; Low, M. J. D. *Chem. Commun.* **1968**, 203.
(32) Nakamura, M.; Mochizuki, Y.; Usami, K.; Itoh, Y.; Nozaki, T. *Solid State Commun.* **1984**, *50*, 1079.
(33) Kaiser, W.; Keck, P. H.; Lange, C. F. *Phys. Rev.* **1956**, *101*, 1264.
(34) Hrostowski, H. J.; Kaiser, R. H. *Phys. Rev.* **1957**, *107*, 966.
(35) Morrow, B. A.; Cody, I. A. *J. Phys. Chem.* **1973**, *77*, 1465.
(36) Hoffman, P.; Knözinger, E. *Surf. Sci.* **1987**, *188*, 181.
(37) Wovchko, E. A.; Camp, J. C.; Glass, Jr., J. A.; Yates, Jr., J. T. *Langmuir* **1995**, *11*, 2592.
(38) Iler, R. K. *The Chemistry of Silica*; Wiley: New York, 1979.
(39) Pimentel, G. C.; McClellan, A. L. *The Hydrogen Bond*; W.H. Freeman: San Francisco, 1960.
(40) Zhou, X.-L.; Flores, C. R.; White, J. M. *Appl. Surf. Sci.* **1992**, *62*, 223.